Supplementary Information

From Co to Co@Co_2P and CoP nanorods: synthesis and performances in phenylacetylene selective hydrogenation

Brandon Azeredo[a], Jason Nguyen-Cong[a], Mathieu Vidal[b], Seema Shafiq,[a,b] Thi Thiet Vu[a], Beatrice Muzzi[a], Audrey Marty[a], Yuanyuan Min[a], Fabio Ferrari[a], Fabien Delpech[a], Céline Nayral[a], Pier-Francesco Fazzini[a, c], Thomas Blon[a], Philippe Serp*[b],[d] Guillaume Viau*[a] and Katerina Soulantica*

[a] Laboratoire de Physique et Chimie des Nano-Objets (LPCNO) UMR 5215, Université de Toulouse, INSA, UPS, CNRS, 135 avenue de Rangueil, Toulouse F-31077, France.
[b] Laboratoire de Chimie de Coordination (LCC) UPR 824, Université de Toulouse, Toulouse INP, CNRS LCC, composante ENSIACET, 4 allée Emile Monso, Toulouse F-31030, France .
[c] CEMES-CNRS, Université de Toulouse, CNRS, 29 rue Jeanne Marvig, 31055 Toulouse, France
[d] Institut Universitaire de France (IUF), France

Table S1. Dimensions of naked nanorods used for the phosphidization reactions.

Length of starting Co NRs L_m (nm)	Diameter of starting Co NRs d_m (nm)	Phosphidized NRs	L_m (nm)	d_m (nm)
61.2 ± 7.7	4.1 ± 0.3	**Co-$P_{0.2/165}$** **Co-$P_{0.7/165}$**	60.2 ± 6.3 60.7 ± 6.0	4.2 ± 0.4 4.8 ± 0.5
68.5 ± 7.5	4.1 ± 0.5	**Co-$P_{0.5/250}$**	na	na
62.7 ± 8.5	4.2 ± 0.4	**Co-$P_{3/165}$**	65.5 ± 8.3	5.4 ± 0.5
71.6 ± 7.3	4.3 ± 0.4	**Co-$P_{3/250}$**	na	6.4 ± 0.6

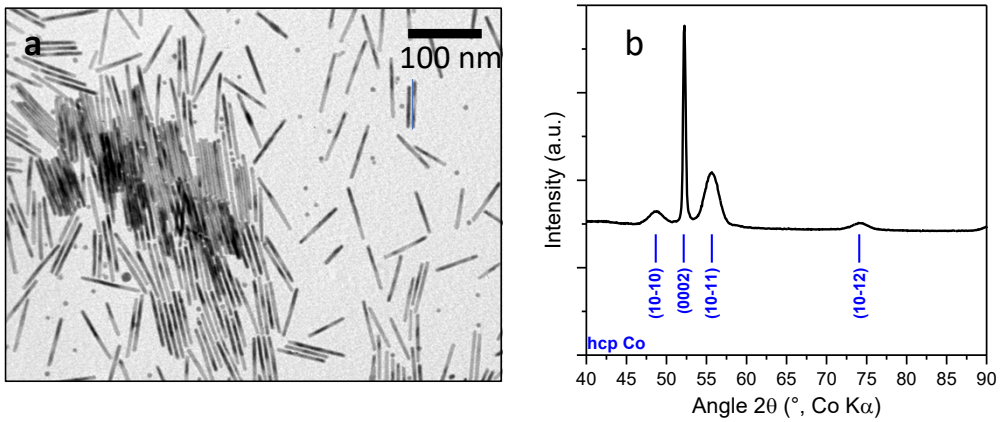

Figure S1. Naked Co NRs (a) TEM image; (b) DRX diffractogram. The blue vertical lines correspond to the expected reflections of *hcp* Co structure (COD file 9008492, $P6_3/mmc$, a=2.507 Å, c=4.068 Å).

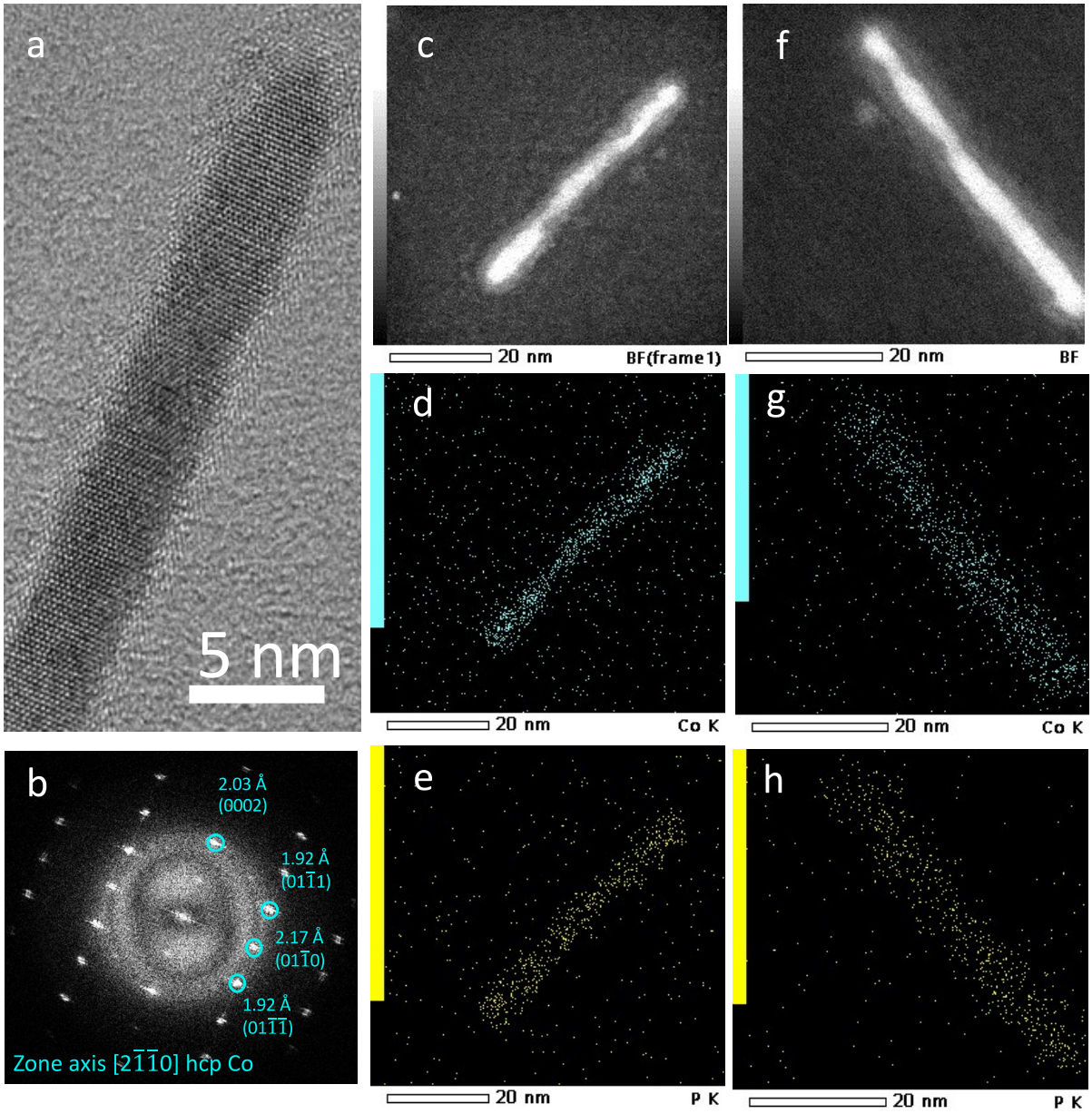

Figure S2. Co-$P_{0.2/165}$: (a) HRTEM, (b) FFT and the corresponding spots of whole NR part shown in (a), (c) STEM-HAADF, (d, e) EDX maps of Co (cyan) and P (yellow); **Co-$P_{0.7/165}$:** (f) STEM-HAADF, (g, h) EDX maps of Co (cyan) and P (yellow).

Table S2: ICP and VSM derived evaluations of the phosphidization degree of the samples

Entry	Sample	Reaction time (min)	*Ms* $_{300K}$ ($A.m^2.kg^{-1}$)	*Ms*-derived Co^0 (wt% / gat%)[a]	ICP Co (wt%/gat%)	ICP P (wt%/ gat%)	P in Co_2P (gat%)[b]	Composition % (Exp.)	Composition % (Theor.)[c]
1	**Co**		134.1	83.7 / 1.42					100 Co
2	**Co-$P_{0.2/165}$**	90	59.2	37.0 / 0.63	61.4 / 1.04	5.96 / 0.19	0.21	60.6 Co / 39.4 Co_2P	60 Co/40 Co_2P
3	**Co-$P_{0.7/165}$**	90	24.1	15.1 / 0.26	64.9 / 1.10	17.1 / 0.55	0.42	23.6 Co / 76.4 Co_2P	100 Co_2P
4	**Co-$P_{0.5/250}$**	180	10.2	6.4 / 0.11	63. 8 / 1.08	15.5 / 0.5	0.48	10.2 Co / 89.8 Co_2P	100 Co_2P
5	**Co-$P_{3/165}$**	180	3.3	2.1 / 0.04	69.5 / 1.18	17.4 / 0.56	0.57	3.4 Co / 96.6 Co_2P	100 Co_2P
6	**Co-$P_{3/250}$**	180	1.3	0.8 / 0.01	52.4 / 0.89	22.2 / 0.72		1.4 Co / 98.6 CoP	100 CoP

a: The Co^0 content was calculated by considering the *Ms* value of the sample at 300 K and dividing it by the *Ms* value of bulk Co (160 $A.m^2.kg^{-1}$).
b: This value was calculated by using the relation: $x_{Co} = y_{Co(0)} + z_{Co2P}$ where x_{Co} are the total gat (gram-atoms) of Co in the sample, derived by the ICP analysis of the sample, $y_{Co(0)}$ are the metallic Co gram-atoms derived from the *Ms* values of the sample and z_{Co2P} are the Co gat of the Co_2P phase. Considering that the P gat incorporated in the Co_2P phase are equal to ½ of the Co gat of the Co_2P phase we can calculate the P gat in Co_2P and the experimentally evaluate the extent of the phosphidization reaction. This value is in good agreement with the ICP-derived P gat.
c : values calculated considering a 100 % yield of phosphidization according to the starting molar ratio (considering exclusively the phases experimentally evidenced in each sample).

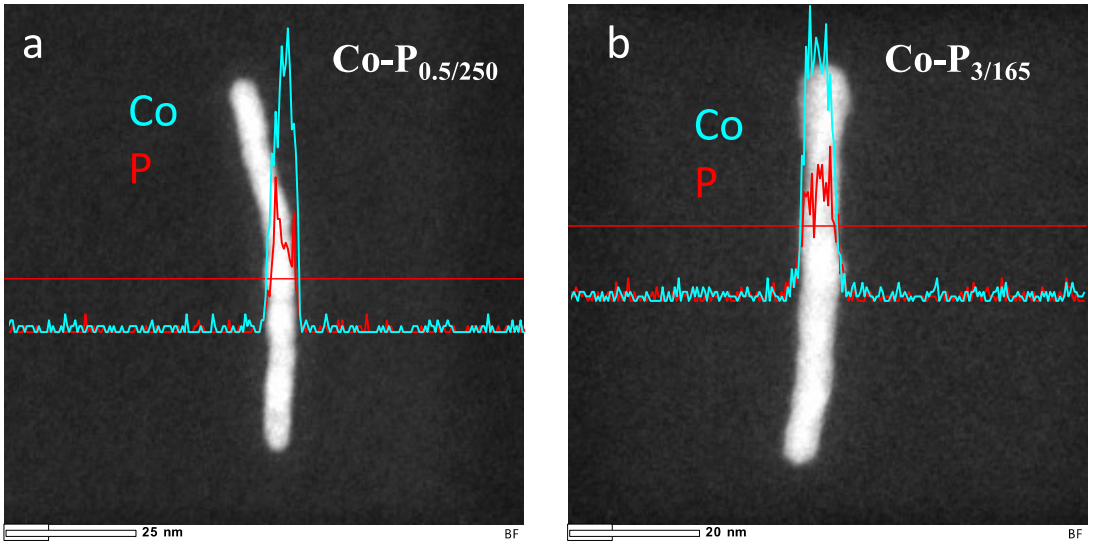

Figure S3. EDX line analysis image of (a) **Co-$P_{0.5/250}$** NRs and (b) **Co-$P_{3/165}$** NRs.

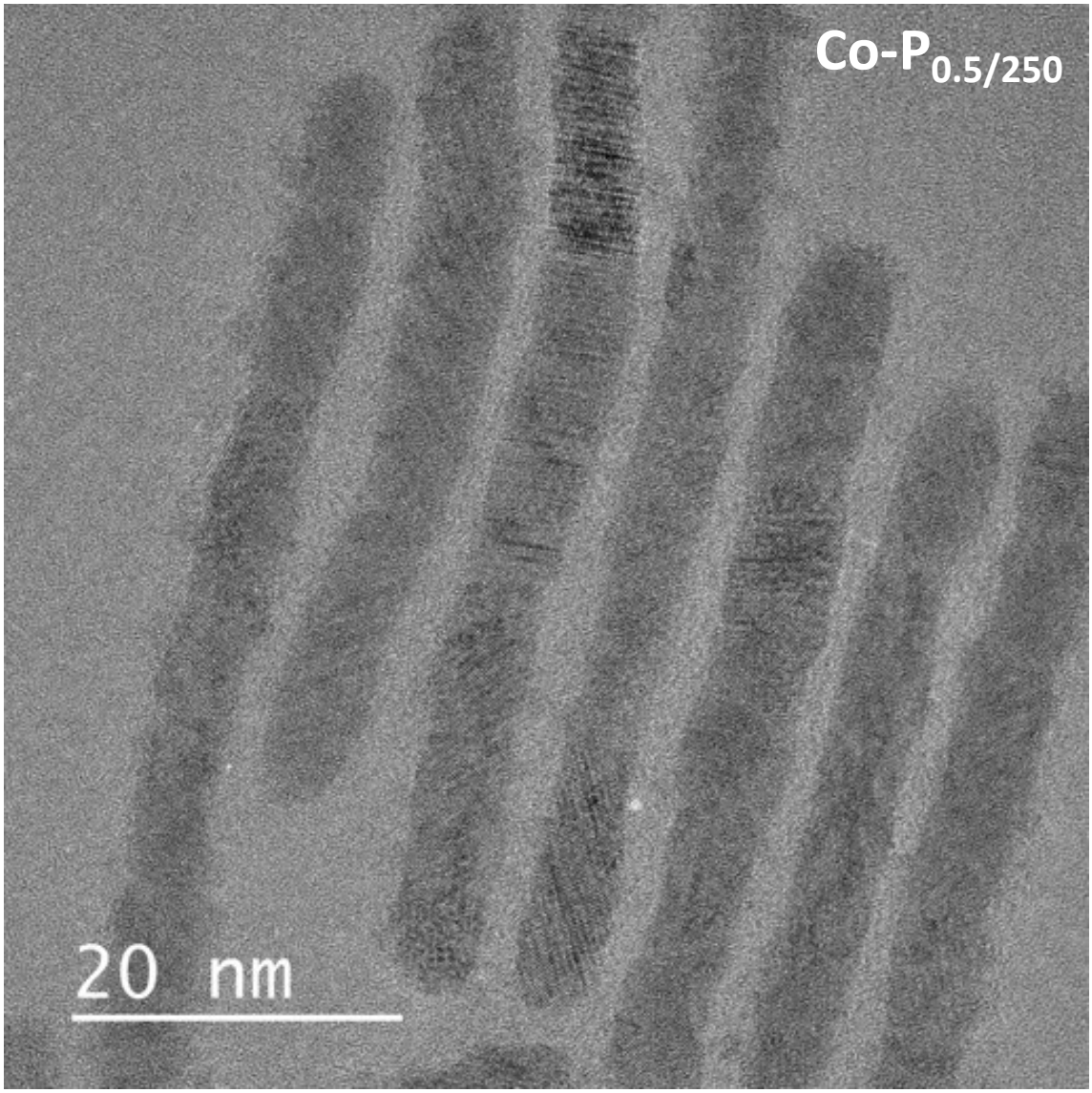

Figure S4. HRTEM images of **Co-$P_{0.5/250}$** NRs. The contrast change and the different orientation of the lattice planes in different regions of the NR indicates that the NR are polycrystalline.

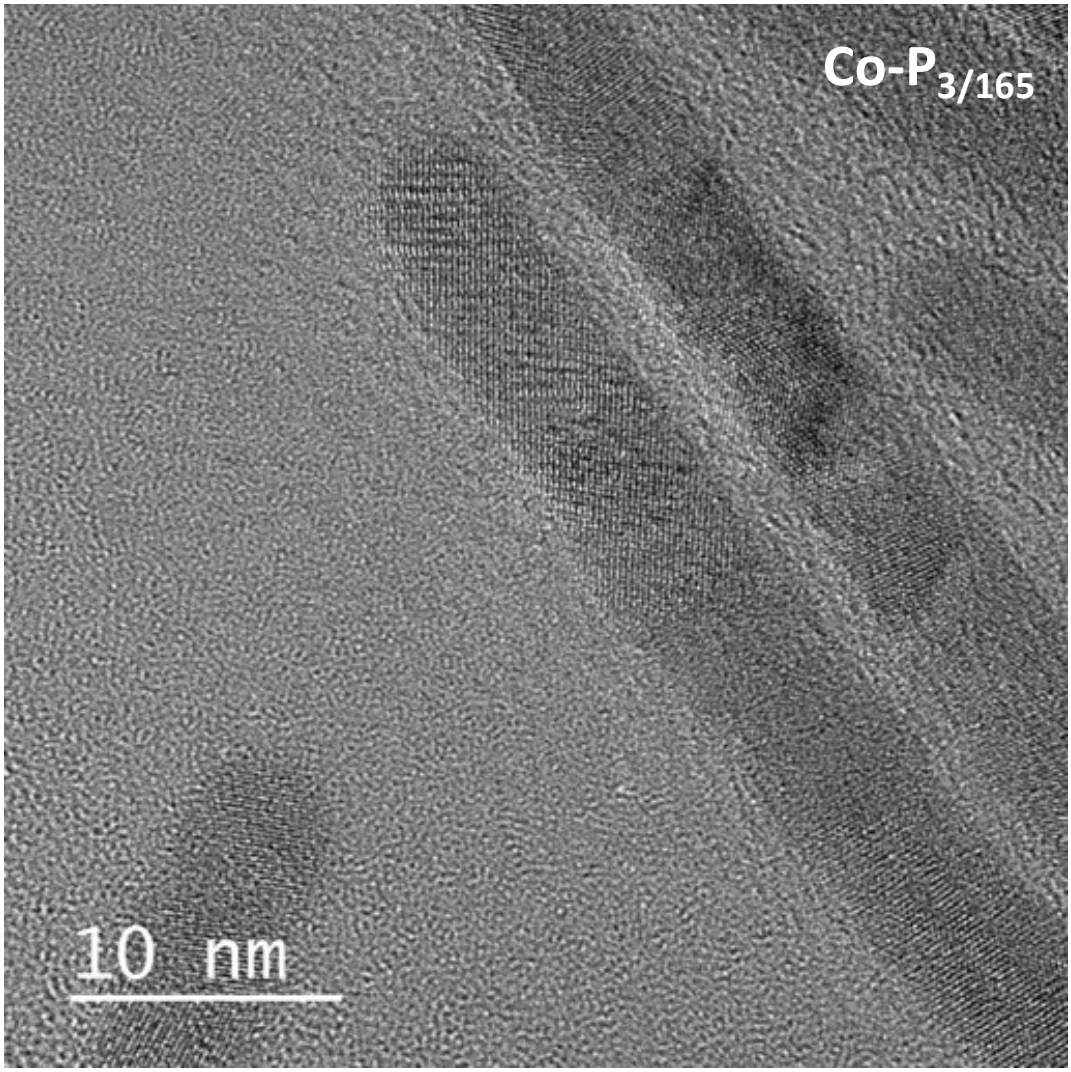

Figure S5 HRTEM images of**Co-P$_{3/165}$** NRs. The contrast change and the different orientation of the lattice planes in different regions of the NR indicates that the NR are polycrystalline.

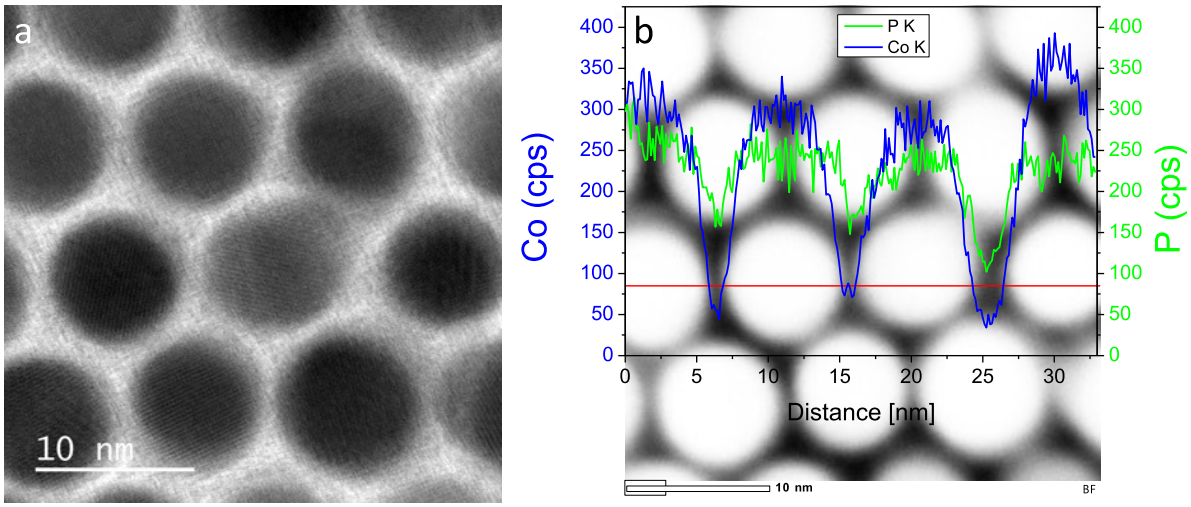

Figure S6. An assembly **Co-P$_{3/250}$** nanorods oriented perpendicularly to the grid and the electron beam: (a) bright field image; (b) Overlay of an EDX line analysis on a HAADF image (blue: intensity of Co characteristic peaks; green: intensity of Co characteristic peaks).

Table S3. Crystal coherence lengths of the main reflections indexed in Fig. 7c obtained by Rietveld analysis of Co-$P_{3/250}$ using MAUD software

h	k	l	d_{hkl}, Å	Cristallite size, nm
1	0	1	3.76	8.6
0	1	1	2.83	8.2
0	0	2	2.80	6.7
2	0	0	2.54	7.5
1	1	1	2.47	9.6
1	0	2	2.45	8,0
2	0	1	2.31	8.2
2	1	0	2.01	10.2
1	1	2	1.96	8.4
2	1	1	1.89	9.9
2	0	2	1.88	8.6
1	0	3	1.75	7.4
0	2	0	1.64	9,0
2	1	2	1.63	9.3
0	1	3	1.62	7.1
3	0	1	1.62	7.9
1	1	3	1.55	7.7
1	2	1	1.50	9.4
2	0	3	1.50	8.3
3	1	1	1.45	9.3

Table S4. ICP-OES and XPS characterizations of the catalysts.

Catalyst	Co/P - at. (ICP-OES)	Co/P - at. (XPS)	Co $2p_{3/2}$ (eV)	P $2p_{3/2}$ (eV)	$Co^{(0)}/CoO_x$
Co-$P_{0.2/165}$	5.5	2.2	778.0 780.4	129.2 132.3	0.5
Co-$P_{0.7/165}$	2.0	1.2	778.2 779.7	129.3 132.3	1.2
Co-$P_{3/250}$	1.2	0.3	778.6 779.6	129.3 132.8	10.2

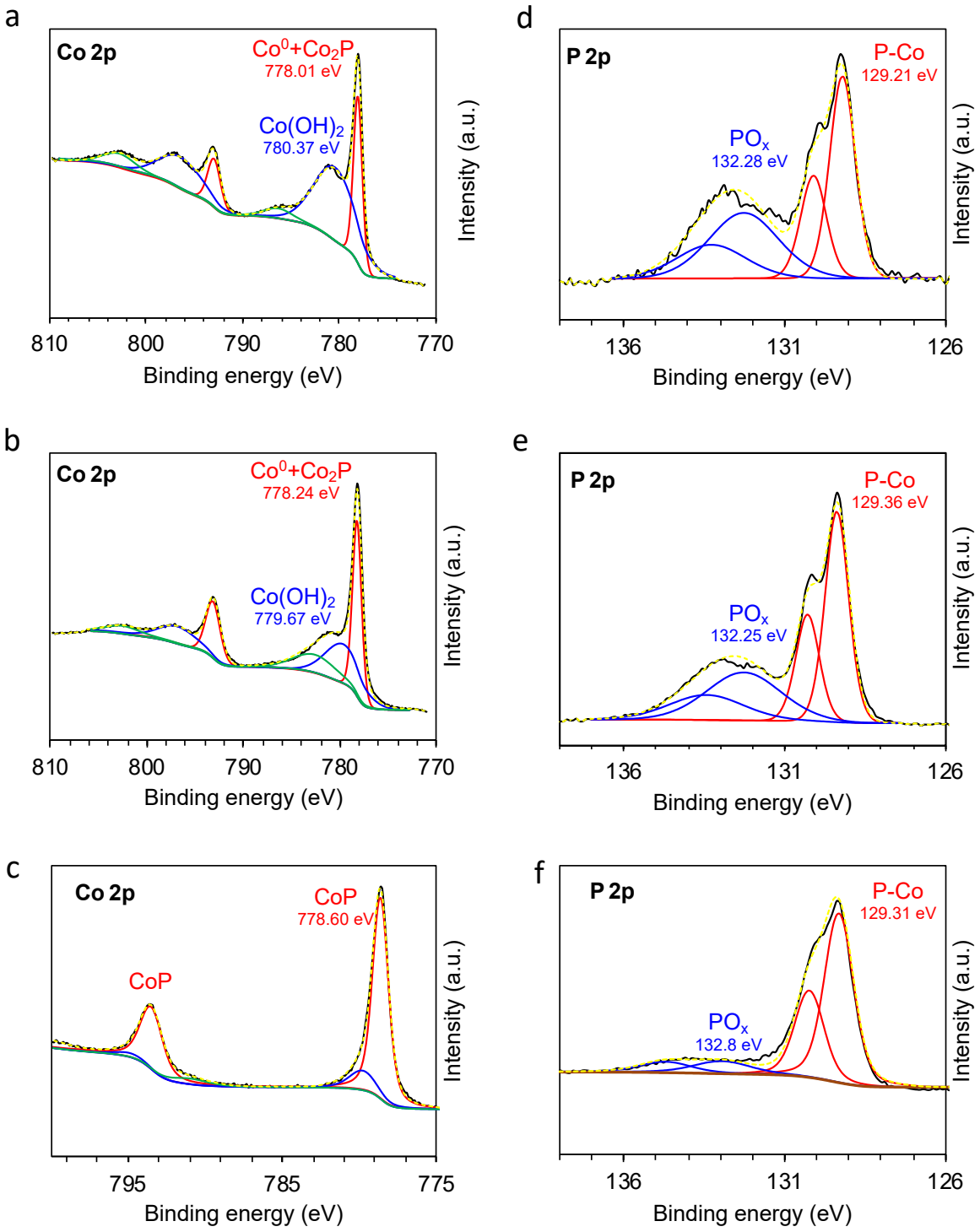

Figure S7. High resolution XPS Co 2p spectra of (a) **Co-P$_{0.2/165}$**; (b) **Co-P$_{0.7/165}$**; and (c) **Co-P$_{3/250}$** NRs. High resolution XPS P 2p spectra of (d) **Co-P$_{0.2/165}$**; (e) **Co-P$_{0.7/165}$**; and (f) **Co-P$_{3/250}$** NRs.

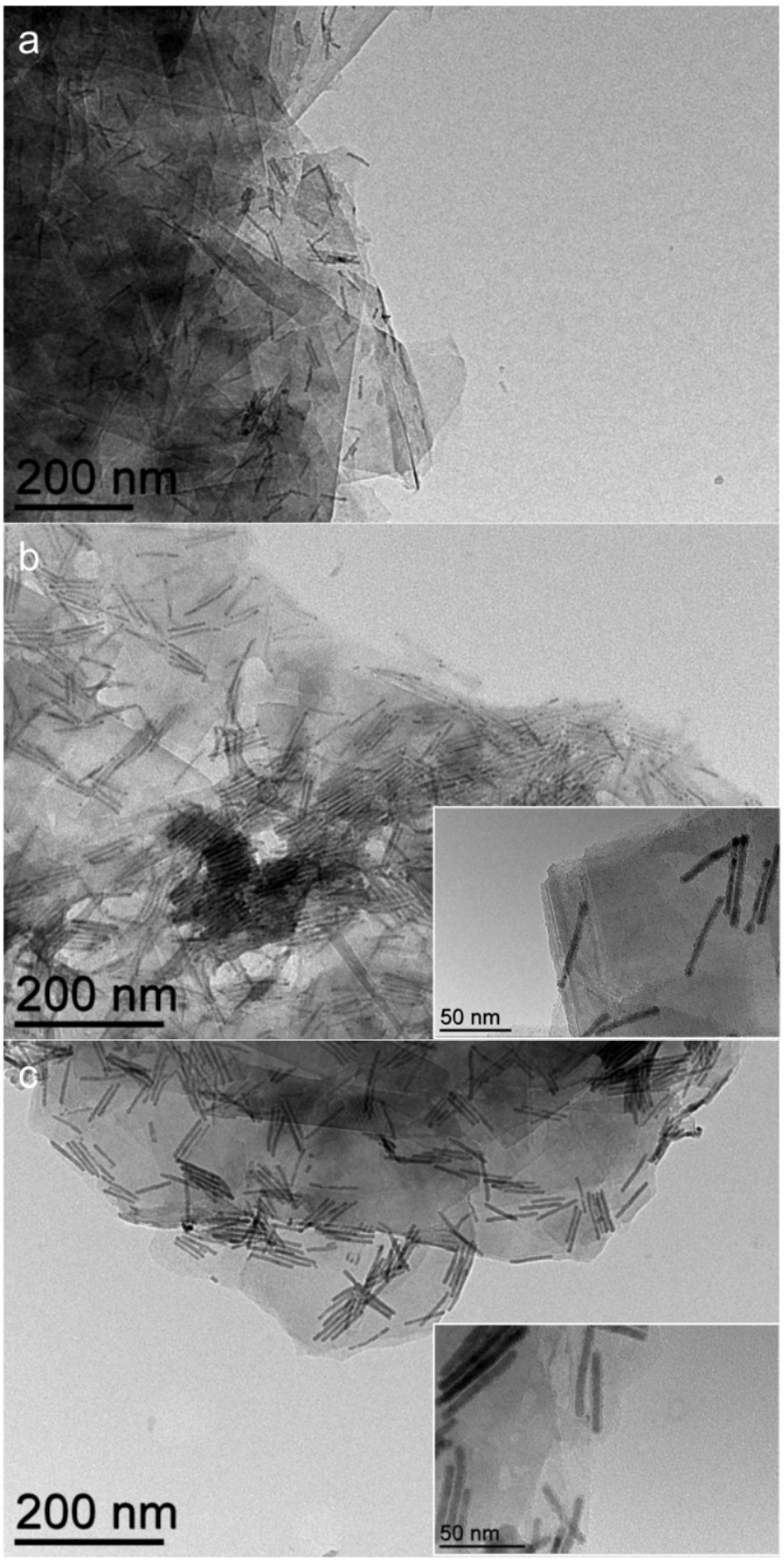

Figure S8. TEM micrographs of (a) Co/FLG; (b) **Co-$P_{0.2/165}$**/FLG; and (c) **Co-$P_{0.7/165}$**/FLG catalysts.

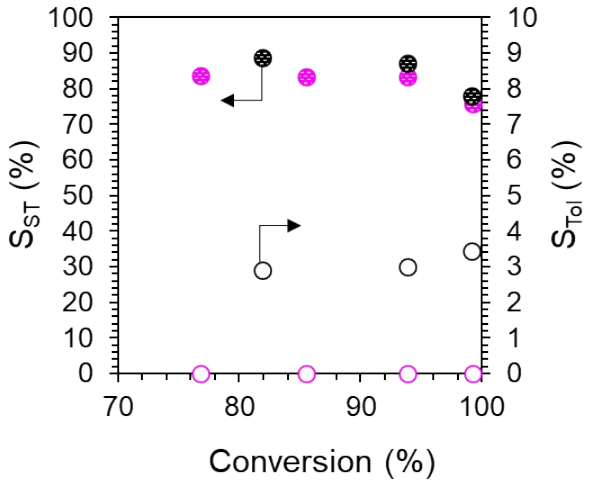

Figure S9. Conversion versus selectivity curves for PhA hydrogenation on unsupported Co NRs (violet circles) and Co/FLG catalyst (black circles).

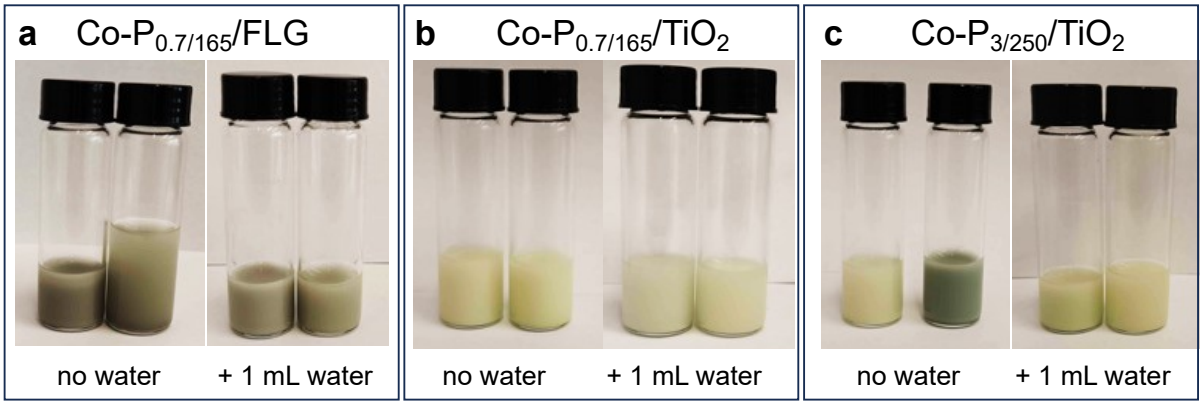

Figure S10. Photographs of 0.1 g of WO_3 mixed with catalysts and treated under the reaction condition in the absence of PhA in the presence or not of water (for each sample and conditions, the left photograph is before test and the right photograph after test. (a) **Co-$P_{0.7/165}$**/FLG catalyst. The grey color is due to the FLG support; (b) **Co-$P_{0.7/165}$**/TiO_2 catalyst; and (c) **Co-$P_{3/250}$**/TiO_2 catalyst.

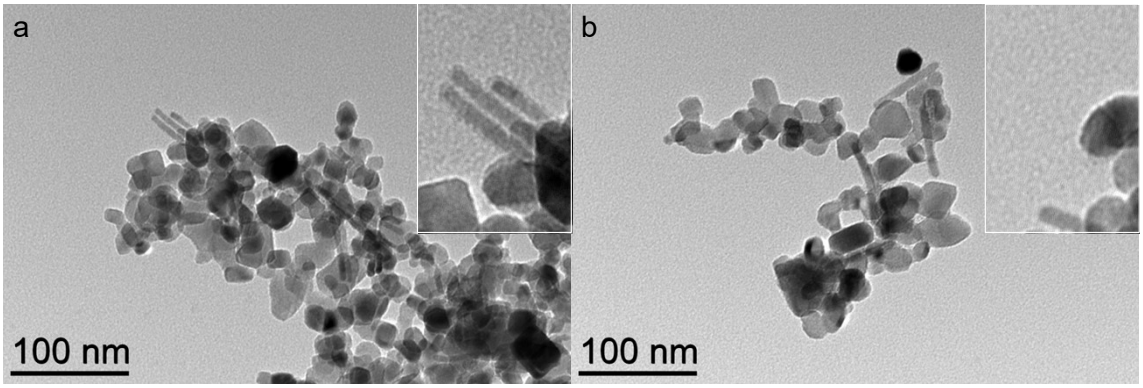

Figure S11. TEM micrographs of the (a) **Co-$P_{0.7/165}$**/TiO_2 and (b) **Co-$P_{3/250}$**/TiO_2 catalysts.

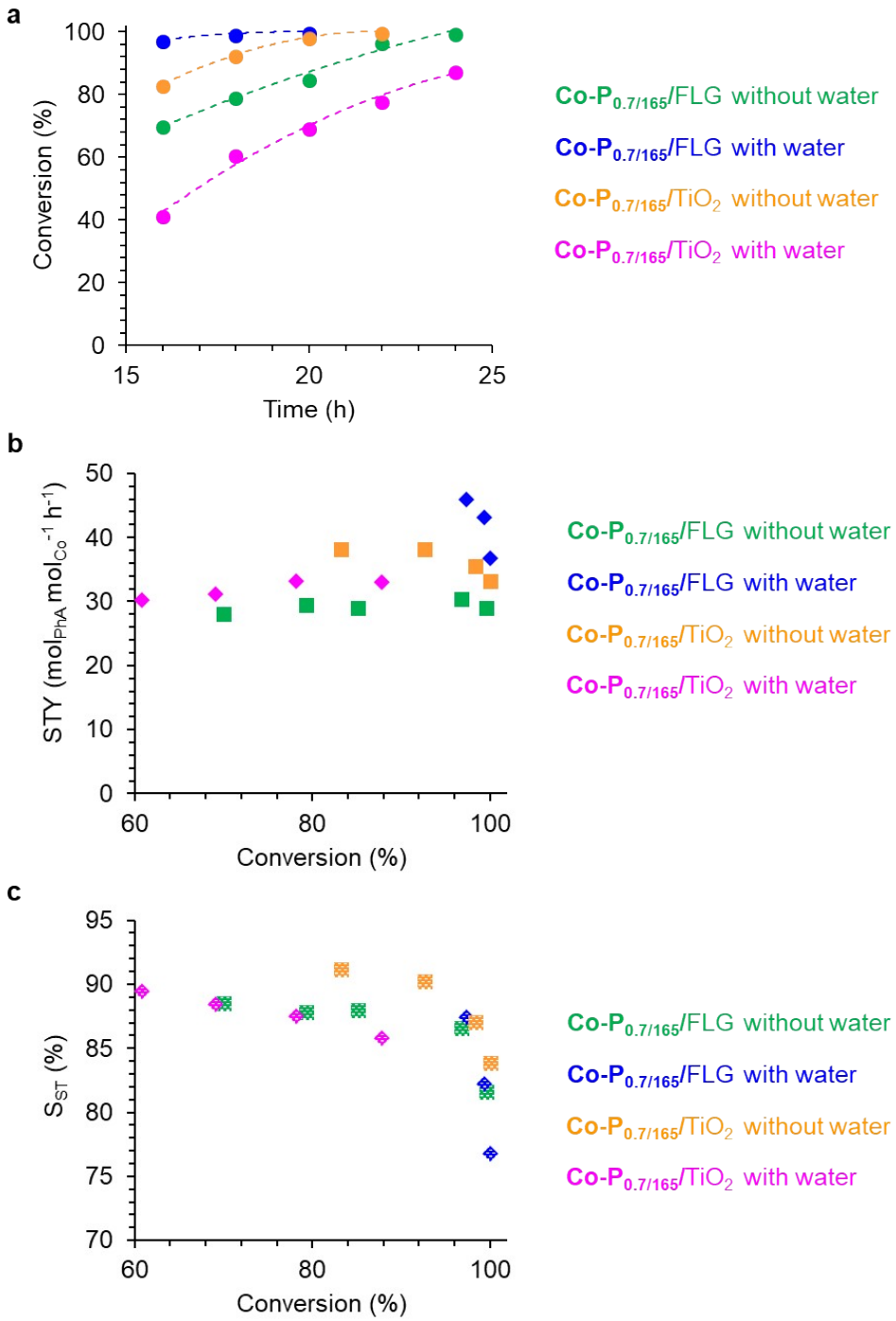

Figure S12. (a) Conversion versus time; (b) activity versus conversion; and (c) selectivity towards styrene versus conversion for the **Co-P$_{0.7/165}$/**FLG without water (green symbols), **Co-P$_{0.7/165}$/**FLG with water (blue symbols), **Co-P$_{0.7/165}$/**TiO_2 without water (orange symbols), and **Co-P$_{0.7/165}$/**TiO_2 without water (orange symbols) systems.

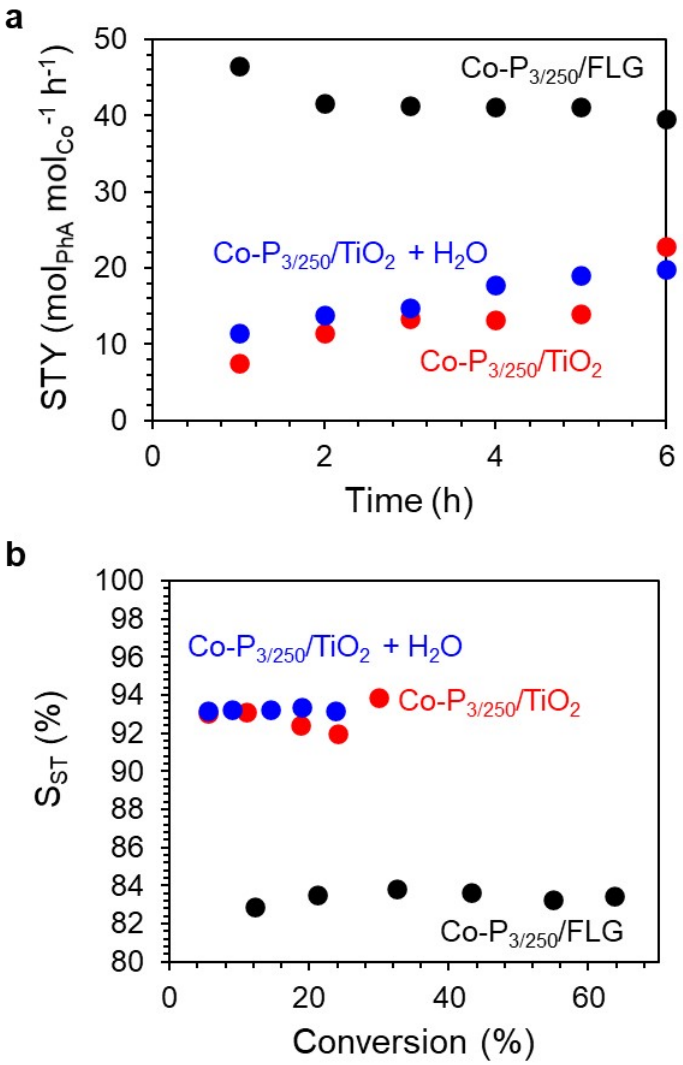

Figure S13. (a) STY versus time of reaction; (b) selectivity towards styrene versus conversion for the Co-$P_{3/250}$/FLG and Co-$P_{3/250}$/TiO_2 (with and without water addition) catalysts.

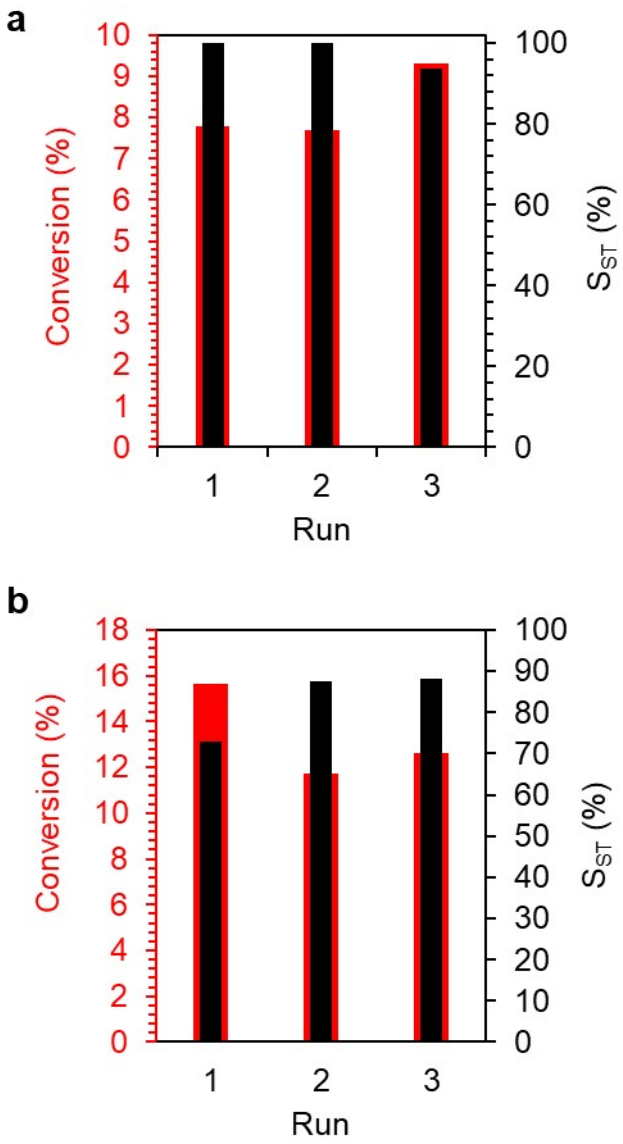

Figure S14. Recyclability tests carried out at 100 °C and 5 bar H_2 for 6 hours on catalysts (a) **Co-$P_{3/250}$/FLG** and (b) **Co-$P_{3/250}$/TiO_2** .

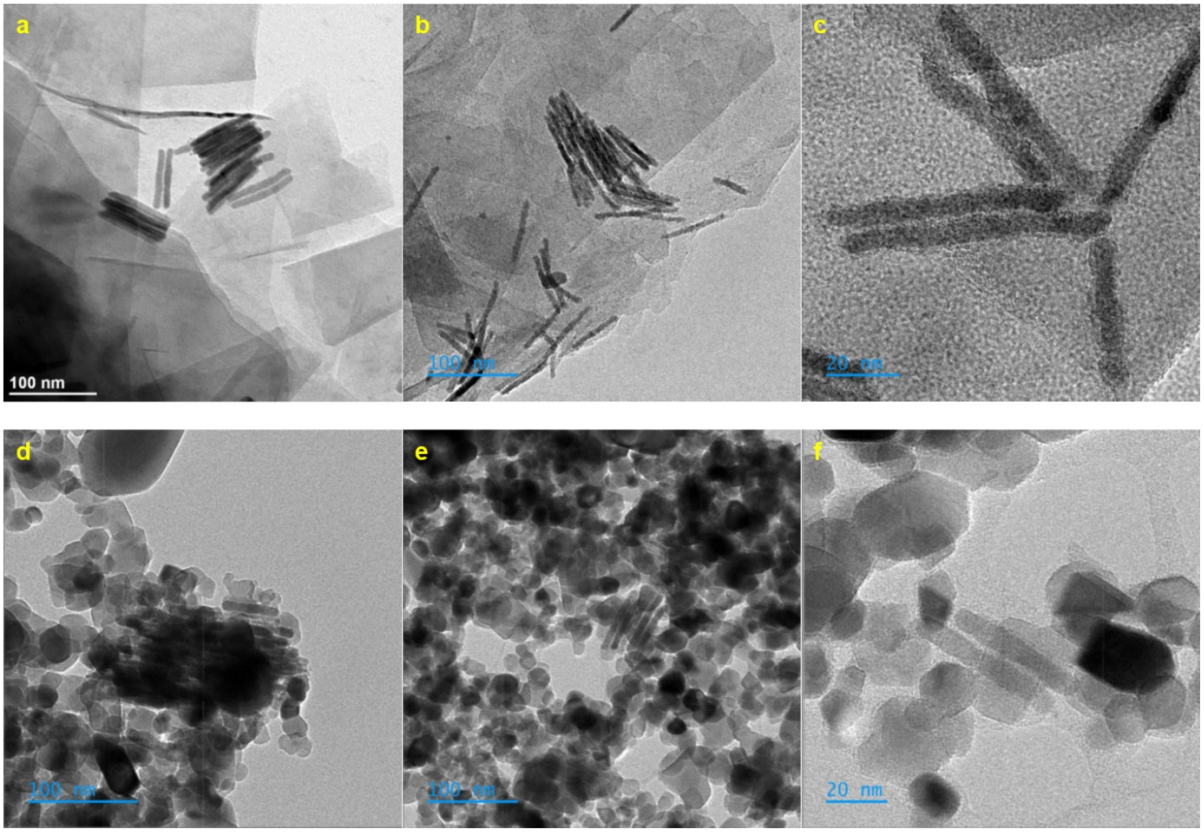

Figure S15. TEM micrographs of (a) the fresh **Co-$P_{3/250}$/FLG** catalyst; (b) and (c) the used **Co-$P_{3/250}$/FLG** catalyst; (d) fresh **Co-$P_{3/250}$/TiO_2** catalyst; and (e) and (f) used **Co-$P_{3/250}$/TiO_2** catalyst. (a), (b), (d), and (e) scale bar = 100 nm. (c) and (f) scale bar = 20 nm.

Table S5. Catalytic performances of metal phosphide catalysts for phenylacetylene hydrogenation.

Catalyst	T (° C)	P_{H2} (bar)	Productivity ($mol_{PhA}\ mol_M^{-1}\ h^{-1}$)	S_{ST} (%)[a)]	Ref.
Ni_2P	85	6	1.67	96 (98 %)	1[1]
Ni_2P/Al_2O_3	100	3	5.5	88.2 (98.6 %)	2[2]
Ni_2P/zeolite	100	10	50.9	93-96 (< 94%)	3[3]
Ni_2P/CNF	100	5	0.02	94.6 (100 %)	4[4]
$Co_{1.2}P$	100	7	0.03	95 (13 %)	5[5]
Co_2P	100	7	0.625	86 (100 %)[b)]	6[6]
$Co\text{-}P_{0.7/165}/TiO_2$	90	5	38	83.9 (100 %)	This work
$Co\text{-}P_{3/250}/TiO_2$	100	5	20	94 (30 %)	This work

a) The number in parenthesis is the conversion at which the selectivity was measured. b) Results obtained in the presence of an additive, tri-n-butylphosphine.

References

1 S. Carenco, A. Leyva-Pérez, P. Concepción, C. Boissière, N. Mézailles, C. Sanchez and A. Corma, *Nano Today*, 2012, **7**, 21–28.

2 Y. Chen, C. Li, J. Zhou, S. Zhang, D. Rao, S. He, M. Wei, D. G. Evans and X. Duan, *ACS Catal.*, 2015, **5**, 5756–5765.

3 W. Fu, L. Zhang, T. Tao and T. Tang, *Journal of Industrial and Engineering Chemistry*, 2021, **95**, 376–387.

4 Z. Guo, Z. Wang and M. Zhang, *Chemical Engineering Journal*, 2023, **463**, 142505.

5 A. Ropp, R. F. André and S. Carenco, *ChemPlusChem*, 2023, **88**, e202300469.

6 A. Ropp and S. Carenco, *Inorg. Chem.*, DOI:10.1021/acs.inorgchem.4c02743.